Electronic Supplementary Information

Electrochemical CO_2 Reduction on Au Surfaces: Mechanistic Aspects Regarding the Formation of Major and Minor Products

Etosha R. Cave, Joseph H. Montoya, Kendra P. Kuhl, David N. Abram, Toru Hatsukade, Chuan Shi, Christopher Hahn, Jens K. Nørskov, Thomas F. Jaramillo*

***Corresponding author:** jaramillo@stanford.edu

1. NMR calibration

Calibration curves of formate and methanol for the ^{1}H NMR spectrum are shown in Fig. S1. Three independent measurements of solutions with known concentrations were fit to a linear trend line.

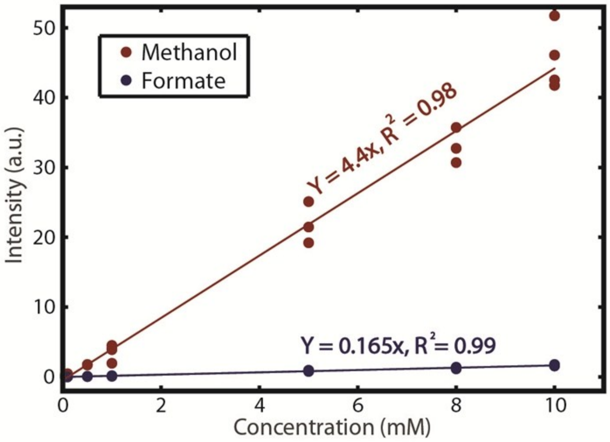

Fig. S1 NMR standards curve for methanol and formate.

2. Surface area measurements

Double-layer capacitance measurements were conducted at various scan rates to measure the ECSA of the sample at various points. The pretreated Au sample and the as-received Au was compared with that of Au deposited on mica, which is considered to have large ordered grains similar to that of a single crystal, and thus is a good representation of flat Au.[1]

The roughness factor (RF) was measured with this technique, and is defined as the ratio of the ECSA to the geometric area of the electrode. Dividing by the aforementioned roughness factors provides a specific activity (per cm^2_{Au}) that can be used to estimate turnover frequencies (TOFs) on a per surface site basis. The as-received Au, which is a polycrystalline foil that has not been exposed to the pretreatment steps outlined in the paper, has an ECSA that is indistinguishable from the Au on mica. This supports the SEM image in Fig. 4a, which shows a relatively flat surface. For the pretreated Au surface prior to CO_2R, a RF of 3 was measured in comparison to the Au on mica as well as the as-received Au. This corresponds to the measured increase in the Au reduction peak, (Fig. 3, CV-3) and the increase in the surface morphology seen in the SEM images of Fig. 4. The RF of the Au surface after CO_2R was 1.33x higher than Au prior to CO_2R as shown in Fig. S2. This implies that although there was some sintering seen via SEM in Fig. 4d, the surface area could have increased slightly. All current density data in this study are reported with respect to the geometric area of the electrode.

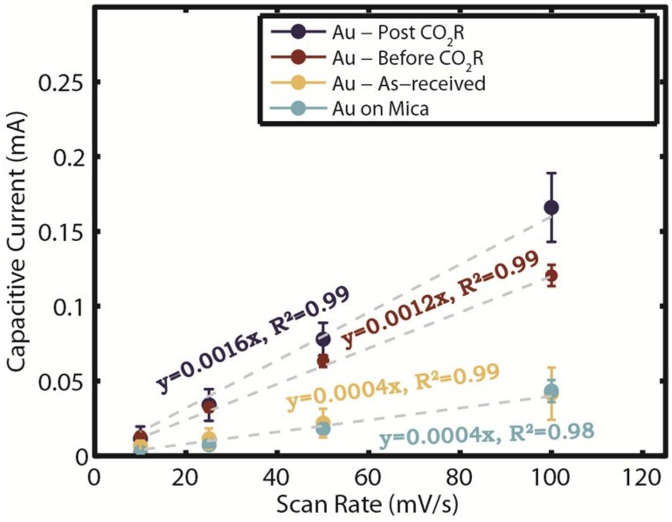

Fig. S2 The capacitive current at a fixed potential versus various scan rates. The slope determined the roughness factor and the ECSA.

3. X-ray diffraction

XRD was used to measure any changes in the phase or orientation of the Au foil at four points in the study: as-received, at point B, at point C and after CO_2R (see Fig. 3). The data shown in Fig. S3, has been normalized to the Au (200) peak, the strongest peak in all samples tested. All of the samples have a comparable ratio of facets, with no apparent shifts due to oxide formation.

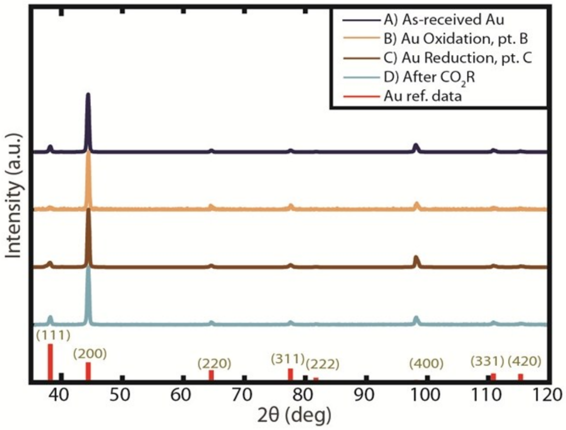

Fig. S3 XRD data for the polycrystalline Au foils at four points in this study.

4. Electrolyte resistance and error analysis

Electrolyte resistance creates a potential drop between the working and the reference electrode. Accounting for this potential drop gives an accurate measurement of the overpotential applied to the working electrode. The potentiostat compensates for this drop in potential by 85%; higher compensation could lead to instability in the instrument. We post-corrected the remaining 15% of the resistance manually after the conclusion of the experiment. The error in this resistance measurement was calculated as the standard deviation of multiple measurements taken throughout a given experiment.

To ensure accuracy, each potential was repeated at least 3 times. The mean and the standard deviation of the corrected potential, the current densities, and the current efficiencies are reported in Table S1.

		Current Efficiency (%)			
E [V] vs. RHE	**I (mA x cm^{-2})**	**CO**	**H_2**	**Formate**	**Methanol**
-0.40 ± 0.002	-0.39 ± 0.08	77.78 ± 10.34	4.84 ± 2.69	4.05 ± 2.52	
-0.54 ± 0.004	-1.84 ± 0.37	82.98 ± 8.32	1.51 ± 0.80	0.08 ± 0.16	
-0.68 ± 0.004	-3.39 ± 0.59	97.01 ± 3.72	2.95 ± 1.64	0.37 ± 0.50	
-0.82 ± 0.010	-4.70 ± 0.28	73.82 ± 11.45	10.48 ± 2.99	0.13 ± 0.16	
-0.96 ± 0.016	-5.78 ± 0.70	66.55 ± 3.66	32.08 ± 9.57	0.94 ± 0.53	0.01 ± 0.01
-1.00 ± 0.014	-7.93 ± 0.46	54.67 ± 6.24	35.22 ± 11.90	0.57 ± 0.06	0.03 ± 0.05
-1.07 ± 0.016	-9.84 ± 0.20	40.58 ± 7.66	65.35 ± 2.32	0.72 ± 0.03	0.07 ± 0.02
-1.14 ± 0.021	-12.89 ± 2.16	25.23 ± 3.19	76.96 ± 7.77	0.55 ± 0.13	0.05 ± 0.02

Table S1 Mean ± SD of applied potentials, total currencies and current efficiencies.

5. CO_2 mass transport limitations

To elucidate the mass transport limitations of CO_2, higher flow rates of CO_2 were tested as shown in Fig. S4a. More moles of CO_2 were reduced at 70 sccm versus 20 sccm likely due to increased transport of CO_2 to the electrode. Fig. S4b shows the total moles of CO_2 reduced as a function of potential for the various metals tested in the cell at 20 sccm.

For Au, Zn, and Ag, the number of CO_2 moles reduced reaches a maximum and even starts to decrease as the overpotential is increased, which is characteristic of mass transport limitations. Additionally, the Au, Zn, and Ag samples reach a similar maximum number of moles reduced, around 4.5 x 10^{-4} moles of CO_2. This behavior is also characteristic of a mass transport limitation of the reactant. In contrast, Cu and Ni do not reach 4.5 x 10^{-4} moles and therefore the amount of reduced moles of CO_2 continues to increase as the overpotential increases. It is therefore hypothesized that at large overpotentials with active metals in this particular electrochemical cell, the transport of CO_2 can limit CO_2R activity as opposed to the inherent kinetic limitations of the specific catalyst. Furthermore, a detailed analysis of the mass transport in this electrochemical cell was performed by Singh et. al. and confirms that the transport of CO_2 limits the CO_2R activity at high overpotentials.[2]

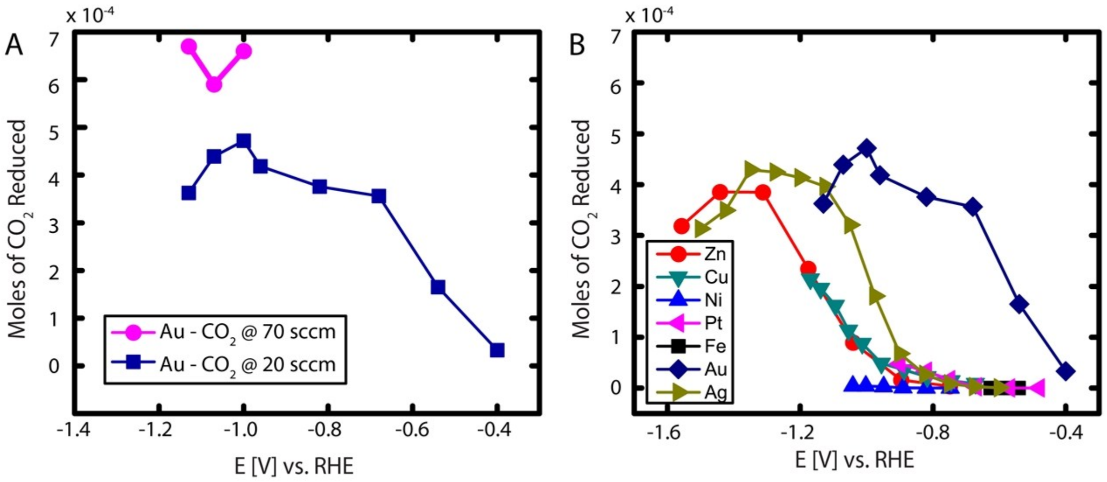

Fig. S4 A) Moles of CO_2 reduced on Au at 70 sccm and 20 sccm flow rate. B) Moles of CO_2 reduced for the various metals used in this electrochemical cell.

6. CO_2R on as-received Au

Another question that may exist is: does as-received Au produce methanol from CO_2 electroreduction or is the oxidative pretreatment a necessary step? To answer this question, we tested an as-received Au foil (no oxidative pretreatment) for two hours and extended the NMR collection time for enhanced sensitivity. At -1.08 V, we observed a 0.01% current efficiency for methanol on the as-received Au, in comparison to the 0.07% current efficiency at -1.07 V, which was measured on the pretreated Au. While a statistically significant difference across multiple potentials was not identified, this qualitative difference could imply that the roughening of the pretreated Au surface may be correlated to the methanol selectivity.

7. $^{13}CO_2$ electroreduction and other CO_2R experiments

$^{13}CO_2$ electroreduction was used to confirm the liquid products were produced from CO_2 as opposed to another carbon source. As shown in Fig. S5, the ^{13}C induces additional splitting of the protons in the formate and methanol. The ^{12}C peaks in Fig. S5 are attributed to the $^{12}CO_2$ that dissolved out of the bicarbonate electrolyte, which was initially present in the solute and not purged out by the $^{13}CO_2$.

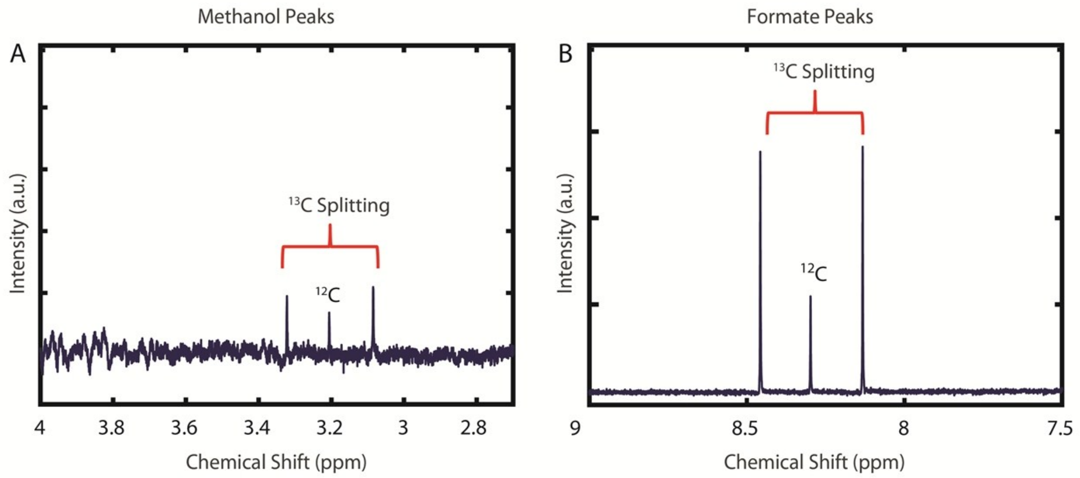

Fig. S5 ^{1}H NMR spectra of $^{13}CO_2$ electroreduction.

In a separate experiment, the Pt counter electrode was exchanged for a Au counter electrode. This experiment was designed to explore the possibility of Pt contaminating the Au working electrode through Pt dissolution and subsequent plating on the working electrode. Similar CO_2R activity and selectivity was observed when the Au counter electrode was used instead of Pt, ruling out any significant impact of the presence of Pt on the system.

Furthermore, a CO_2R experiment was performed without the anion exchange membrane present to ensure the products detected were from the reduction of CO_2 and not from the degradation of the membrane. Similar products were detected when compared to experiments with a membrane present.

8. Extended CO_2 electroreduction on Au

Five-hour long chronoamperometry was performed on a Au sample (Fig. S6). The electrolyte in this experiment was sampled once per hour. The methanol partial current density remained steady, which implies continuous formation of methanol over the five hours. It is also worth noting the product formation on Au for all four products is fairly stable versus time as illustrated in Fig. S6.

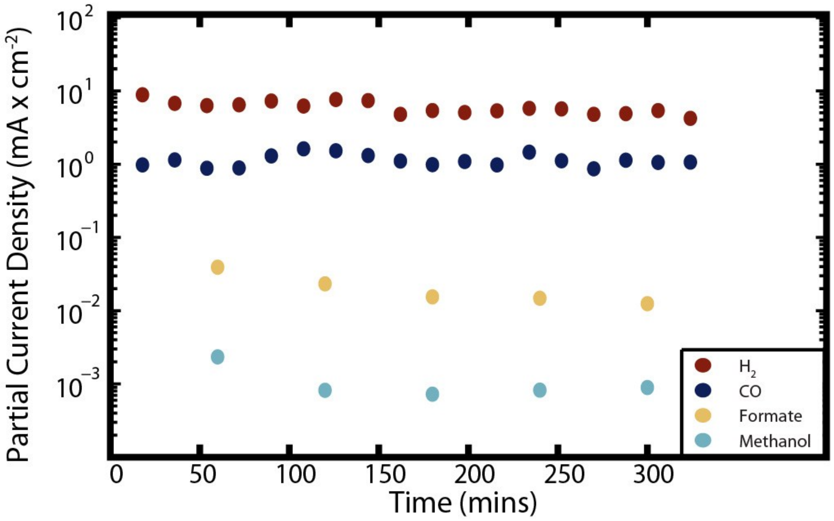

Fig. S6 Partial current density for CO_2 electroreduction on Au for five hours at -1.1 V.

9. Formate reduction on Au

Formate has been shown to reduce to methanol on certain metals.[3] An experiment was run to see if methanol detected during CO_2 electroreduction could be coming from readsorbed formate. One-hour long chronoamperometry was performed at -1.2 V in an argon-saturated solution of 0.1 M potassium formate and 0.1 M $KHCO_3$. No methanol was detected.

10. DFT Calculations

Density functional theory calculations presented herein were carried out on a 3x3x3 slab representing the (211) surface of Au using the Dacapo calculator and the open-source atomic simulation environment (ASE) software package.[4] Adsorbates and the top layer of the slab were geometrically relaxed for each binding site, and the most stable adsorbate configuration was used to determine the electronic component of the free energy. Corrections to the free energy from the harmonic approximation were used,[5] along with a solvation correction of 0.25 eV for species with pendant hydroxyls (i.e. $^*CH_2OH$, $^*CHOH$) and 0.1 eV for adsorbed $^*CO$, as per previous work.[6] The revised Perdew-Burke-Ernzerhof (RPBE) functional was used for its accuracy in describing adsorption energies[7] and a 4x4x1 Monkhorst-Pack k-point mesh.[8] Parameters of 340 and 500 eV were used for plane wave and density cutoff energies, respectively, with a Fermi-level smearing width of 0.1 eV.

11. References

1. C. E. D. Chidsey, D. N. Loiacono, T. Sleator and S. Nakahara, *Surf. Sci.*, 1988, **200**, 45-66.
2. M. R. Singh, E. L. Clark and A. T. Bell, *Physical Chemistry Chemical Physics*, 2015, **17**, 18924-18936.
3. S. Kapusta and N. Hackerman, *J. Electrochem. Soc.*, 1983, **130**, 607-613.
4. S. R. Bahn, K. W. Jacobsen, S. R. Bahn and K. W. Jacobsen, *Am. Inst. Phys.*, 2002, **4**, 56-66.
5. C. J. Cramer, *Essentials of Computational Chemistry: Theories and Models*, Wiley, 2nd edn., 2004.
6. A. A. Peterson, F. Abild-Pedersen, F. Studt, J. Rossmeisl and J. K. Norskov, *Energ. Environ Sci.*, 2010, **3**, 1311-1315.
7. B. Hammer, L. B. Hansen and J. K. Nørskov, *Phys. Rev. B.*, 1999, **59**, 7413-7421.
8. H. J. Monkhorst and J. D. Pack, *Phys. Rev. B.*, 1976, **13**, 5188-5192.